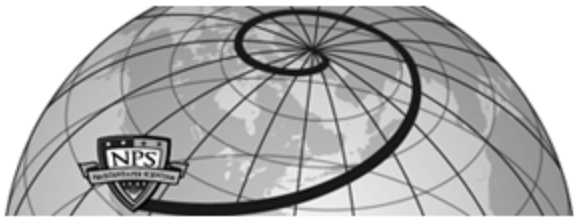

DESIGN AND CONSTRUCTION OF A MODIFIED RAYLEIGH REFRACTOMETER FOR THE TWO-TO-12 MICRON INVESTIGATION OF VAPORS

JAMES D. KNIPP
and
STANLEY LENARD

DESIGN AND CONSTRUCTION OF A MODIFIED RAYLEIGH REFRACTOMETER FOR THE TWO-TO-12 MICRON INVESTIGATION OF VAPORS

by

James D. Knipp
Captain, United States Army

and

Stanley Lenard
Captain, United States Army

Submitted in partial fulfillment of
the requirements for the degree of

MASTER OF SCIENCE
IN
PHYSICS

United States Naval Postgraduate School
Monterey, California

1 9 6 3

DESIGN AND CONSTRUCTION OF A MODIFIED RAYLEIGH REFRACTOMETER FOR THE TWO-TO-12 MICRON INVESTIGATION OF VAPORS

* * * * *

James D. Knipp

and

Stanley Lenard

DESIGN AND CONSTRUCTION OF A MODIFIED RAYLEIGH REFRACTOMETER FOR THE TWO-TO-12 MICRON INVESTIGATION OF VAPORS

by

James D. Knipp

and

Stanley Lenard

This work is accepted as fulfilling
the thesis requirements for the degree of
MASTER OF SCIENCE
IN
PHYSICS
from the
United States Naval Postgraduate School

ABSTRACT

A multi-channel Rayleigh refractometer similar to the one constructed by Eaton and Thomas was proposed to investigate the optical dispersion of vapors in the two-to-12 micron region. The proposed system differed from the previous gas measurement system primarily in the methods of vapor admission and pressure-temperature control. Additional modifications included changes in monochromator and source assembly design, provision for two-directional scan of the infrared spectrum, and changes in the interferometer gasketing and end window design.

This report covers the design and construction of such a system by Captain James D. Knipp, USA, and Captain Stanley Lenard, USA, at the U. S. Naval Postgraduate School from July 1962 through May 1963, at which time the system was completed and ready for operation.

The writers wish to express appreciation to Professor Sidney H. Kalmbach both for his ideas that fostered this project and his guidance throughout its pursuit.

TABLE OF CONTENTS

LIST OF ILLUSTRATIONS

TABLE OF SYMBOLS

n	Index of Refraction
λ	Wavelength of incident electromagnetic radiation
λ_1, λ_2	Characteristic absorption wavelengths
m	Number of fringes; or integer
L	Geometrical length of interferometer
T	Temperature, degrees Kelvin
ΔP	Pressure Differential, Vapor minus Vacuum
I	Intensity
β	½ Phase difference across slit of width a, $\beta = \frac{\pi a \sin\theta}{\lambda}$
γ	½ Phase angle of adjacent slits, $\gamma = \frac{\pi d \sin\theta}{\lambda}$
N	Number of slits or channels
a	Slit width
d	Slit distance (distance between centers of adjacent slits)
θ	Angle between the plane of the slit and the normal to the incident radiation
s	Detector slit width
f	Focal length of paraboloidal mirror
$\delta\theta$	Angular halfwidth of principal maxima
W	Distance, edge of mask slit to side of channel
D	Width of channel
g	Exit slit width
R	Resultant amplitude of six slits
R_1	Resultant amplitude of one set of alternate slits
R_2	Resultant amplitude of second set of alternate slits
R_o	Amplitude contribution of one slit
ϕ	Phase difference

I. INTRODUCTION

Although the optical dispersion of gases has long been a subject of study, experimental difficulties have limited investigation in the infrared region. Historically, most of the effective investigations have been conducted using hollow prisms. These instruments gave very accurate measurements of the refractive index although subject to certain systematic errors near absorption bands. Much of the early literature has been collected by Van Vleck /1/, and, more recently, by Jaffe /2/.

In an effort to improve accuracy, investigations in the visible and infrared regions have been conducted at the U. S. Naval Postgraduate School since 1956 using a Rayleigh refractometer (or interferometer). Low radiation intensity with this refractometer limited investigation to three microns; therefore, in 1959, Eaton and Thomas /3/ designed a six-channel Rayleigh refractometer with associated dual manifold vacuum and gas admission system, which extended the range of investigation to twenty-five microns. This apparatus, slightly modified, was used in 1960 by Muncie and Whittemore /4/ to investigate the optical dispersion of carbon dioxide.

These investigations using both modified and unmodified Rayleigh refractometers determined the refractive indices of gases; i.e., substances which exist in the vapor phase at room temperature. The gas admission systems were designed

accordingly, and no temperature regulation of the refractometer was required during operation. A system, built around a six-channel Rayleigh interferometer, was therefore designed specifically for investigation of the optical dispersion of vapors; i.e., substances which exist in the liquid phase at room temperature. This system incorporates both close regulation of the interferometer temperature, and an appropriate vapor admission system; its design and construction is the subject of this report.

II. GENERAL

a. Optical Dispersion of Vapors

The term "optical dispersion" refers to the variation with frequency of the refractive index of a material. Gas (and vapor) molecules, consisting of separated positive and negative charges, can be considered as an assemblage of oscillating dipoles which emit electromagnetic radiations of one or more frequencies corresponding to the oscillatory mode or modes of the atom. A molecule having N atoms has 3N degrees of freedom; of these, three degrees of freedom are translational, three (or less, depending upon the symmetry of the molecule) are rotational, and the remainder are vibrational. Each of these vibrational degrees of freedom has its own characteristic vibrational frequency. When electromagnetic radiation is passed through the vapor, the varying electric fields of the incident waves impress forced vibrations upon the molecules of the vapor. At incident wave frequencies approaching a characteristic vibrational frequency of the vapor molecule, the amplitude of the forced vibrations of the vapor molecules becomes large. So much of the energy of the incident wave is removed to produce this large-amplitude vibration that the vapor exhibits strong absorption. This is known as resonance absorption, and has an acoustical analogy in the sympathetic vibrations of a tuning fork (acoustic resonance).

The refractive index n has been found to depend on the wavelength λ of the incident light. In spectral regions remote from absorption bands, the refractive index of a substance decreases regularly with increasing wavelength. This is referred to as normal dispersion, and n may be represented in these regions by the empirical Cauchy formula

$$n = A + B/\lambda^2 - C/\lambda^4 ,$$

where A, B, and C are constants characteristic of the substance concerned.

Near an absorption band the index n begins to decrease more rapidly than is indicated by the Cauchy formula. A better dispersion formula has been given by Sellmeier:

$$n^2 - 1 = A\lambda^2/(\lambda^2 - \lambda^2_o),$$

where A is a constant and λ_o is the wavelength at which maximum absorption occurs. If a substance has more than one absorption band, this equation becomes

$$n^2 - 1 = \sum_s A_s \lambda^2/(\lambda^2 - \lambda^2_o),$$

where the summation has to be taken over all the relevant absorption bands (Figure 1).

It should be noted that this dispersion formula indicates a discontinuity in n at λ_o, which is contrary to observation. In practice, an additional term in the denominator (due to damping) precludes discontuity at λ_o. Through an absorption band the refractive index drops to a finite minimum value,

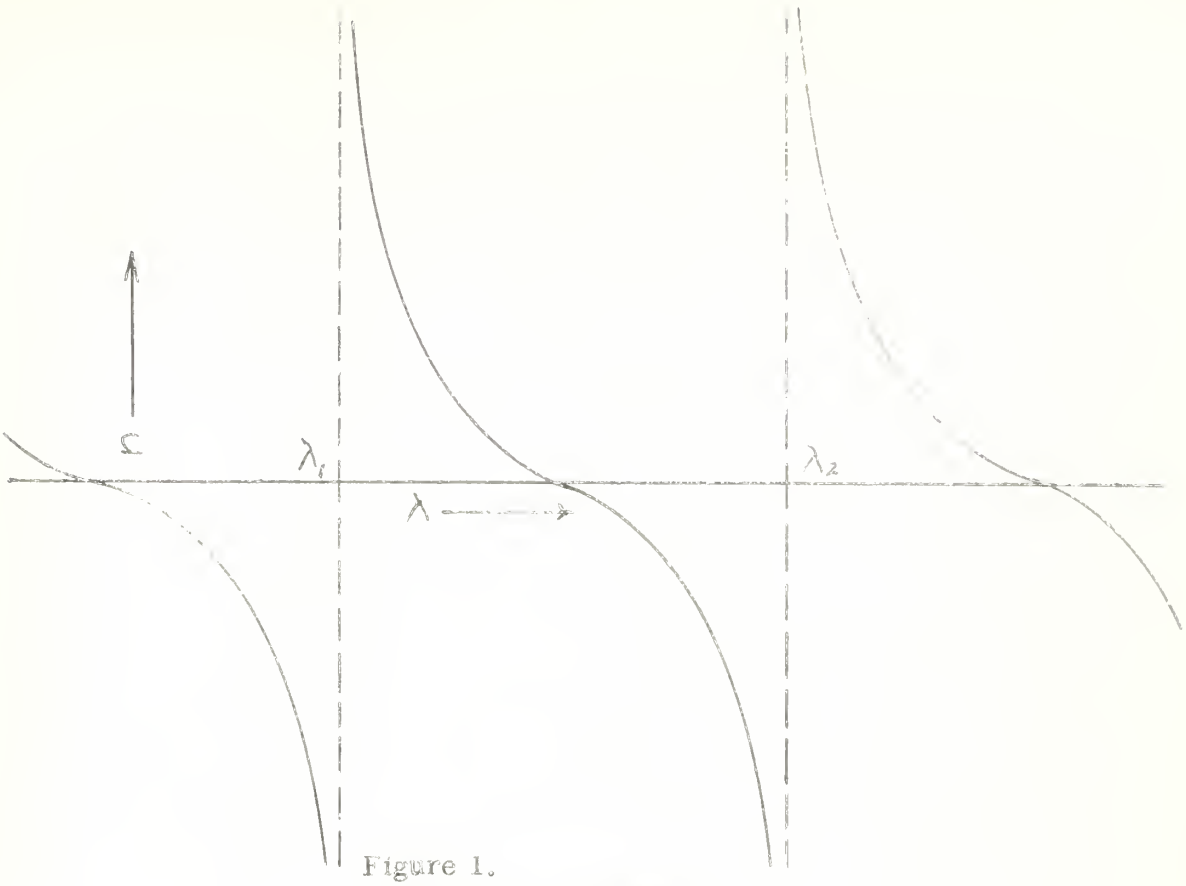

Figure 1.
Dispersion as predicted
by Sellmeier formula

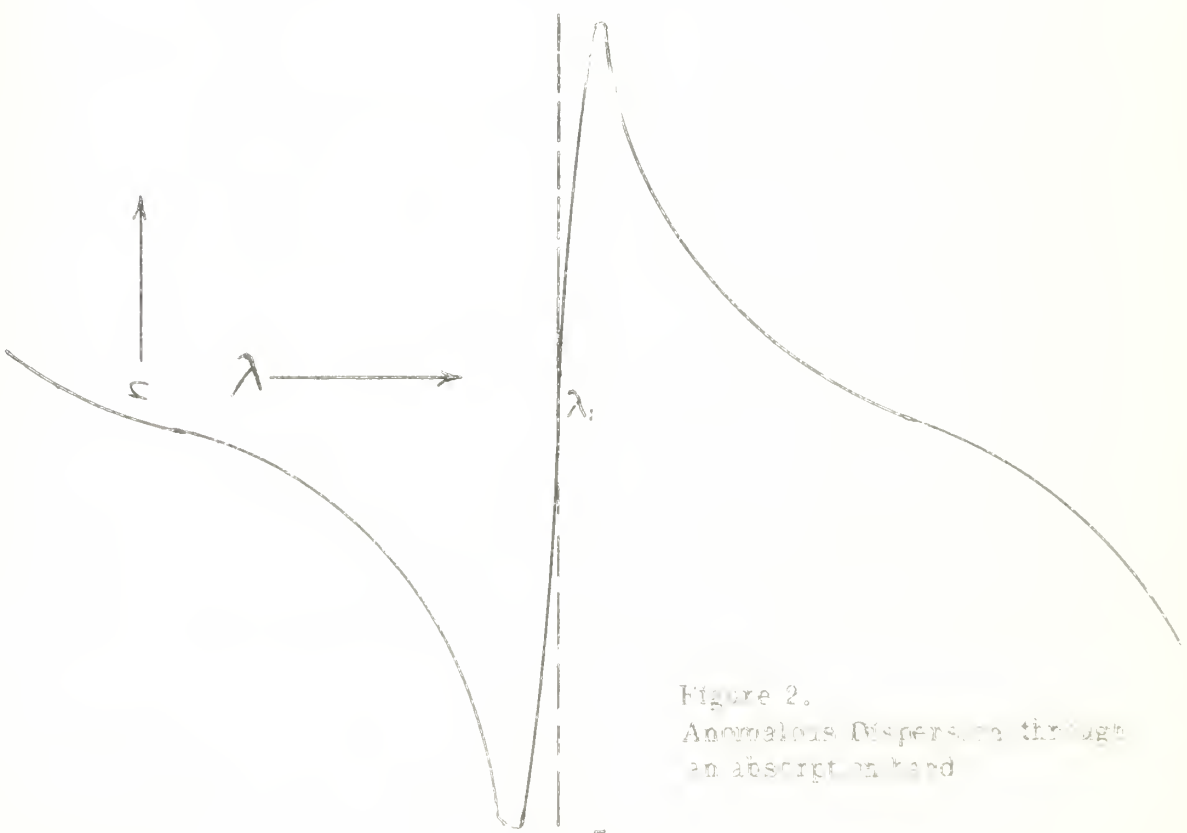

Figure 2.
Anomalous Dispersion through
an absorption band

rises steeply to a maximum value, and then decreases again as indicated in Figure 2 . This increase of n with increasing wavelength is called "anomalous dispersion", although it is normal inside an absorption band. /2/

b. Interferometric Determination of Refractive Index.

By dividing a collimated monochromatic beam of light into two parts, then recombining the parts to form interference maxima and minima, an interferometer provides a means of measuring refractive indices. By passing the split beam through two different media of the same geometrical length, it is possible to determine the difference in optical path lengths by interpretation of the observed fringe pattern as this optical path length is varied. "The Rayleigh Refractometer is by far the most accurate and convenient means available of measuring small changes of refractive index." /5/

The modified Rayleigh Refractometer constructed for this study was designed to measure the index of refraction of a vapor with respect to a vacuum. This is accomplished by passing one half of the incident beam through a vacuum, while the other half of the beam is passed through channels into which the vapor is being admitted. As the vapor flows into the refractometer, the optical length of the vapor-containing channels increases, and the fringe pattern shifts. This shift manifests itself as alternate intensity maxima and

minima passing laterally across a detector slit which is so adjusted that no part of more than one maximum (or minimum) can be observed.

The basic equation for determining the difference between the refractive indices of two media is:

$$n_1 - n_2 \cong \frac{m\lambda}{L}$$

This reduces to $n-1 \cong \frac{m\lambda}{L} \frac{T}{273.16} \frac{760}{\Delta P}$ for correcting the index of refraction of the vapor to 0°C and 760 mm Hg pressure with respect to a vacuum /6/.

c. The Advantage of Multiple Channels

The Rayleigh refractometer, by dividing collimated energy into two parts and then rejoining the beams to form interference patterns, should be an excellent means of measuring the refractive index of a gas or vapor. In practice, however, it has been found that low radiation intensity hinders fringe detection, particularly at long wavelengths. It is therefore necessary either to increase the radiation intensity of the source, or to modify the instrument. Since the increase in intensity required for fringe resolution is beyond the capability of the Globar source used in this construction, a modified Rayleigh interferometer similar to that designed by Eaton and Thomas /3/ was adopted.

The intensity of the principal maximum of a Fraunhofer diffraction pattern of N slits of equal width, each equally spaced, is given by the formula

$$I = I_o \frac{\sin^2\beta}{\beta^2} \quad \frac{\sin^2 N\gamma}{\sin^2\gamma}$$

(see Table of Symbols for meaning of symbols used). For small angles of the phase angle γ, I is proportional to N^2. It is this increase in intensity with the square of the number of slits that fostered the idea of a multi-channel interferometer.

In order to maintain the proper phase relationship between radiation travelling in the separate vacuum and vapor channels and still have recombination in the proper maxima and minima, the manifolding for the vacuum and vapor admission system was designed so that one set of alternate channels were evacuated, with the other set of channels containing the vapor under investigation. The interferometer, therefore, is essentially three two-channel interferometers built side by side so that the maxima and minima of their diffraction patterns reinforce each other.

The phase relationships of radiation from alternate slits are developed mathematically in Appendix III.

III. EQUIPMENT

a. General Description

The equipment assembled for this investigation is as follows (see also Figures 11 through 16):

1. A source assembly built around a globar and a 13 cps chopper.
2. A Perkin-Elmer, Model 98, Monochromator, with quartz and sodium chloride prisms, modified to deliver a collimated beam to the refractometer.
3. A modified Rayleigh refractometer.
4. A detector assembly to focus the infrared energy from the refractometer on a lead sulfide or a thermocouple detector.
5. A Perkin-Elmer Model 107 amplifier which amplifies and feeds into the recorder (see f below) the signal received from the detector preamplifier.
6. A modified Leeds and Northrup Speedomax Recorder, Type G, to provide a graphical record of the energy intensity reaching the detector.
7. A vacuum system, adequate to maintain and measure the desired vacuum, built around a Cenco HYVAC 7 forepump and a Pirani Vacuum Gauge.
8. A gas desorption system connected to the vacuum system.
9. A vapor admission system which allows vapor to enter the appropriate channels of the interferometer.

b. Modified Rayleigh Interferometer

The modified Rayleigh interferometer was patterned closely after that constructed by Eaton and Thomas /3/, with primary differences in end window and gasketing materials (Figure 13).

Basically, the interferometer is a rectangular brass tube, with sides, top, and bottom fabricated from one-half inch brass plate. Slots were milled into the top and bottom plates to receive the 16 gauge brass channel partitions. These partitions, when inserted and sealed in place, form the sides of the six parallel channels. Dimensions of the interferometer are as follows:

Length	50 cm
Height	6.0 cm
Width	5.8 cm
Channel height	3.4 cm
Channel width	5.0 mm
Channel spacing, center-to-center	6.0 mm

Throughout the construction of the interferometer special care was taken to insure a good vacuum seal. To achieve this, the slots milled in the top and bottom plates to receive the channel partitions were cut 0.002 inches wider than the channel partitions. Next the slots, partition edges, and joints between top, sides, and bottom were tinned with 50/50

lead-tin solder. The interferometer was then assembled, the top and bottom were loosely attached to the sides with machine screws, and the entire assembly was placed on its side in an oven. Wires of 50/50 lead-tin solder were placed along the tinned joints wherever possible, and the assembly was heated above the solder melting-point. After tightening the screws holding the top and bottom to the sides, the interferometer was allowed to cool, excess solder beading was scraped away, and the ends were machined smooth and parallel.

Flanges were fastened to both ends of the interferometer with machine screws. Two aluminum discs, one attached to each flange with eight bolts, serve to hold the end windows and gasketing material firmly in place. These end windows are three-inch diameter discs one-eighth inch in thickness of Kodak IRTRAN 2, which permit infrared transmission in the two to twelve micron range. Three-mill Teflon sheets with rectangular holes cut to correspond to the channel openings, were lightly coated with stopcock grease and placed between the IRTRAN 2 discs and the interferometer to provide vacuum seal. A thin metal mask, with six slits (see Appendix II for determination of slit width) was attached on the outer surface of one IRTRAN 2 window to provide the proper interference pattern.

Evacuation of and gas admission to the channels of the interferometer is accomplished by means of two manifolds attached to the top plate. These manifolds each cover a

group of three slots cut through to alternate channels. Machine screws and neoprene gaskets make the manifolds vacuum tight.

In operation the interferometer is supported by two wooden legs, each approximately $1\frac{1}{2}$ x 3 inches in cross section. These legs hold the interferometer in a horizontal position on an optical bench, and have adjusting screws to permit tilt adjustment.

The pressure of the water vapor must be known for each experimental run; since this vapor pressure is determined from the vapor temperature, an oven was built around the interferometer to maintain a constant temperature (Figure 15). The framework of the oven was fabricated from wooden strips; one-eighth-inch thick Masonite sheeting was then nailed to both the inside and the outside of this framework to provide a double wall, which was lined with aluminum foil on the inside surface. The oven is heated by heating tapes suspended from horizontal rods within the oven, while thermocouples attached to the outside of the interferometer and suspended both in the water-vapor admission system and in a water-vapor channel of the interferometer itself permit accurate temperature measurement.

The modified Rayleigh interferometer thus constructed is suitable for investigating the optical dispersion, in the near-infrared region, of any vapor that is not corrosive to

the instrument. With proper protective coating (e.g., Glyptal-coating the interior surfaces), this instrument could be used for any vapor for which sufficient vapor-pressure data were available.

c. Vacuum and Vapor Admission System

Vacuum for the system was provided by a Cenco Hyvac-7 forepump. All vacuum lines, with the exception of short rubber vacuum-tube couplings, were constructed of thirteen-millimeter diameter glass tubing, with six-millimeter vacuum stopcocks located appropriately (see Figure 3 for vacuum system schematic).

After leaving the forepump and associated cold trap, the vacuum divides to provide vacuum for both the interferometer and the gas desorption system. The vacuum line going to the interferometer is valved, and then branches to connect to both manifolds of the interferometer. A water trap (designed to contain triple-distilled water during experimental runs) connects to the vacuum line immediately above one interferometer manifold through a standard taper joint to provide the source of vapor. This water trap, and the glass tubing to a level immediately above the standard taper joint, are enclosed by the same oven that contains the interferometer.

For an experimental run, the water trap is connected to the vapor manifold of the interferometer through the standard taper joint (but with water trap stopcock closed),

the oven is closed, and the liquid in the water trap is allowed to attain run temperature. Valves Number One and Two are opened, evacuating both vacuum and vapor channels of the interferometer. To begin the run, energy of a preselected wave length is passed through all six channels of the interferometer. Valve Number One is closed, sealing off the vapor channels and water trap from the remainder of the vacuum system. Next the water trap stopcock is opened slowly so that the number of fringes passing the detector can be counted on the chart recorder. At the completion of the run the water trap stopcock is closed, and Valve Number One is opened to evacuate the vapor channels. Next a different preselected wave length is selected, and the system is ready for another run. This procedure is repeated until the supply of liquid in the water trap is exhausted, at which time the trap is removed, refilled with a few milliliters of purified liquid, and again attached to the vapor manifold of the interferometer.

d. Gas Desorption System

Since the pressure of the vapor in the interferometer is determined indirectly from temperature measurements, rather than from direct measurement of the total pressure in the vapor channels, the presence of contaminating gases would not distort the pressure determination. However, the index of refraction as measured by the refractometer would be a

weighted average of the indices of refraction of the vapor and the contaminants. To preclude this, for optical dispersion investigation of water vapor (the anticipated first operational use of this system), a gas desorption system was built to desorb gases from triple-distilled water prior to its admission into the interferometer. This system consists of a stationary water container capable of being evacuated, (a standard cold trap with a removable outside shell is used), a water trap that also connects to the interferometer during operation (described in preceding section), and associated glass tubing and stopcocks (Figures 3 and 16). The pressure gauge used during interferometer operation to monitor the vacuum channels is so positioned that it is also available for intermittent use with the gas desorption system.

In operation, distilled water is introduced to the system at the stationary water container. Valve Number Three is then opened, and the system is evacuated. Next Valve Three is closed, sealing off the entire system. The stationary water container is next immersed in a hot water bath, the water trap is immersed in an equilibrium mixture of dry ice and acetone, and time is allowed for the water to vaporize and condense (as ice) in the water trap. Valve Number Three is then momentarily opened, allowing the gases desorbed during the preceding step to be swept from the

system. The positions of the hot water bath and cold bath are now reversed, and the water is allowed to sublime into the stationary water container. The desorbed gases are again swept away, and the cycle is repeated until the contaminants are so dilute that they do not distort measurement of the refractive index of the vapor under investigation. The process is stopped with the water in the water trap; by closing the water trap stopcock and venting the desorption system, the water trap can be detached at the standard taper joint and attached to the interferometer for operation (see preceeding section for attachment procedure).

The gas desorption procedure, although thorough, takes considerable time; it is suggested, therefore, that an alternate (and much quicker) procedure be first attempted. This alternate procedure consists of (1) attaching the water trap to the interferometer and admitting the water vapor as for normal operation, (2) closing the water trap stopcock, (3) evacuating the vapor channels by opening Valve Number One, (4) closing Valve Number One, and (5) readmitting water vapor to the vapor channels by opening the water trap valve. Since the solubility of most gases in water is quite low at the operating temperature of the interferometer (90-100° C), this procedure should result in most contaminating gases being swept from the system.

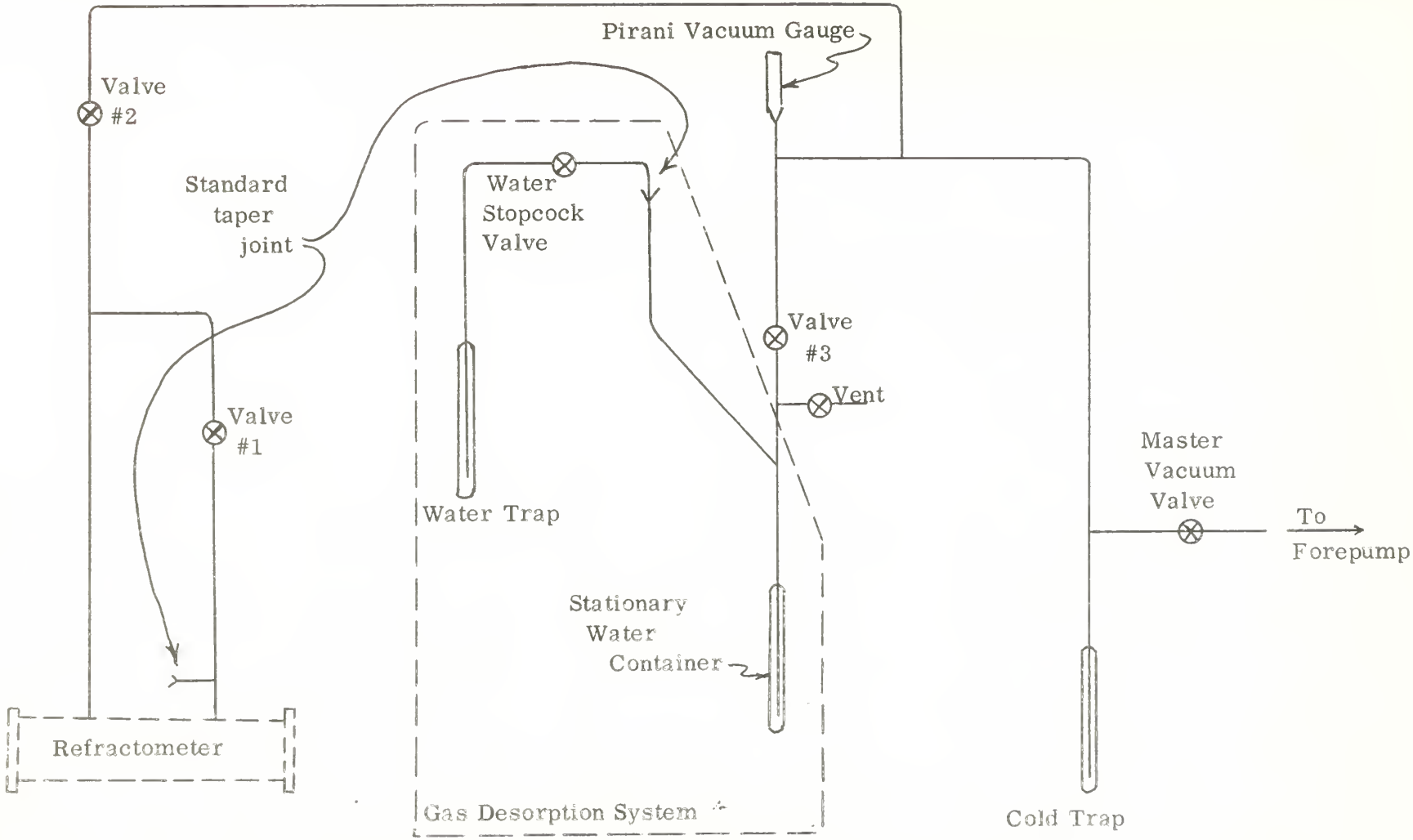

Figure 3. Vacuum and Gas Admission System, Including Gas Desorption System

e. Optical System

The optical system consists of a source assembly, a monochromator, a refractometer, and a detector assembly (Figures 4, 5, and 11).

(1) The source assembly includes a globar emitter in its standard mount; a Chopper Rectifier to chop the globar radiation at 13 cycles per second and rectify the detector signal fed to the amplifier; and two mirrors, M-1 and M-2 to focus the chopped energy on input slit of the monochromator.

(2) The mirrors M-6 and M-7 were mounted on the chassis of a standard Perkin-Elmer Model 98 Monochromator to collimate the monochromatic beam leaving the exit slit S-2 of the monochromator and deliver this beam to the refractometer.

(3) See section b below for a description of the refractometer.

(4) The detector assembly consists of an off-axis parabolic mirror M-8 to focus the energy leaving the refractometer on the adjustable detector slit S-3. This slit which is on an adjustable mount, is located at one focus of the elllipsoidal mirror M-9, and the detector (either lead sulfide or thermocouple) is at the other.

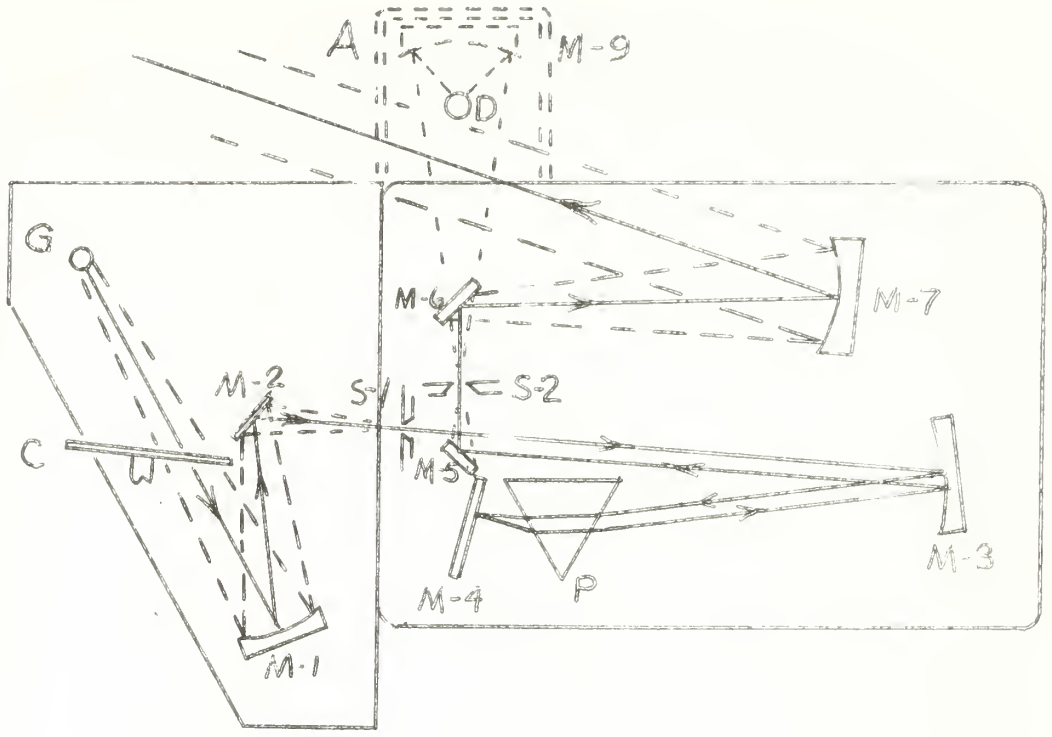

Figure 4. Infrared Source and Monochromator

Legend

G Globar source

C Chopper

M-2, M-5, M-6 } Plane mirrors

M-3, M-7 } 18°-off-axis parabolic mirrors

P Prism

M-4 Littrow mirror

S-1 Monochromator input slit

S-2 Monochromator output slit

A Recommended calibration platform, including:

M-9 Ellipsoidal mirror

D Detector

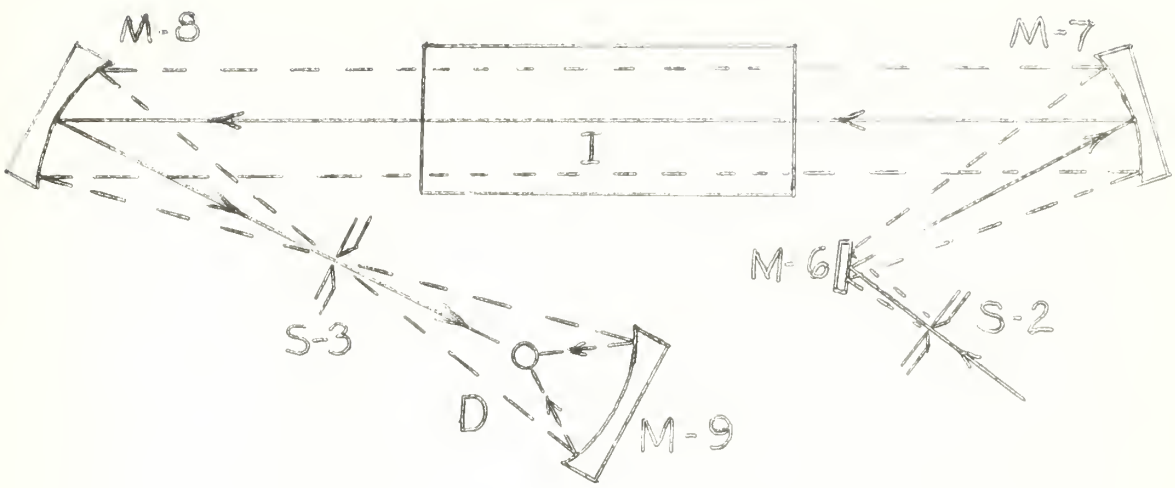

Figure 5. Interferometer Optical System

Legend

S-2	Monochromator exit slit
M-6	Plane mirror
M-7, M-8	18°-off-axis parabolic mirrors
I	Interferometer
S-3	Detector slit
M-9	Ellipsoidal mirror
D	Detector

f. Experimental Measurements

Significant repetitive measurements taken during this study were relative intensity of transmitted energy, vacuum, vapor temperature, and wave drum settings.

(1) A Speedomax Recorder, was used to display variations in the intensity of the energy falling on the detector.

(2) A Pirani Vacuum Gauge was used in checking the vacuum and vapor admission system and the interferometer for satisfactory seal. In further work, it is to be used to monitor the vacuum side of the interferometer during experimental runs for determining refractive indices of vapors.

(3) Three Iron-Constantan thermocouples and a potentiometer were used to measure the temperature at three points in the system. Thermocouple junctions were located:

(a) inside the water trap,

(b) in the center of the centermost vapor channel in the refractometer, and

(c) on the outer surface of the refractometer.

The oven and its contents were brought up to temperature by use of three electrical heating tapes plugged into a terminal whose voltage was controlled by a variac. Under evacuated conditions, it was not possible to obtain the same potentiometer reading (thus temperature) at all three points. Due to lack of time, no attempt was made to ascertain whether use of water in the trap and water vapor in the

refractometer vapor channels would give the same reading on all three thermocouples.

(4) A microswitch was connected to the amplifier to mark desired predetermined wave drum locations on the recorder during a calibration run. These marks were made by manually depressing the switch as the desired wave drum settings were passed.

IV OPERATION

a. System Checks and Optical Alignment

Vacuum was applied to the main vacuum line, and each segment of the system was checked separately to insure satisfactory seal. The refractometer was tested with one manifold open to the atmosphere while vacuum was applied at the other; then this procedure was reversed. Extended periods of degassing at an elevated temperature (86°C) were required before the solder flux constituents were removed from the interior surfaces of the refractometer.

The entire system was assembled in final configuration and tested for attainable vacuum as well as ability to maintain a vacuum once the forepump was valved off. The pressure in the system rose 10 microns in 30 minutes in the final test.

The monochromator was optically aligned with a mercury source using procedures outlined in Perkin-Elmer Manuals. Then mirrors M-6 and M-7 (Figure 4) were mounted so that the output beam was collimated, the fine adjustment of M-7 being controlled through an image of the input slit seen through a telescope. Next the source assembly was built and so aligned that the light from the source was focused on the input slit of the monochromator. When it was found that a mercury pencil source fits inside the globar housing, good adjustments could be made. At this point the source assembly plate was

firmly attached to the monochromator, and the entire assembly was mounted so that the collimated beam of monochromatic light leaving mirror M-7 passed properly through the refractometer. Then the detector assembly was located and brought into alignment, with focus being visually checked and obtained with the help of various paper screens. The alignment procedures outlined in the Perkin-Elmer manuals were found adequate.

The electronic components were then checked according to instructions contained in manuals furnished with the equipment, and the amplifier was peaked at 13 cps. It was found that phasing of the chopper-rectifier is much easier and faster when the oscilliscope is not used as it is impossible to obtain the test patterns shown in the manuals with oscilloscopes available here.

Once all optical and electronic components were functioning properly the optical alignment was rechecked and fine focus was achieved by maximizing the detector signal displayed on the recorder with the monochromator slits set at 20 microns.

b. Wave Drum Calibration

The position of the wave drum determines the wave length of the radiation passing through the monochromator. The circumference of the wave drum is scale divided so that any one setting is reproducible; however, the wave drum must be calibrated against known absorption spectra so that the wave

length emitted at a given wave drum setting is known. This is accomplished by

(1) turning the wave drum at a constant speed (i.e., "scanning" the Globar emission spectrum),

(2) passing the monochromatic beam through a gas or film with a known absorption spectrum,

(3) recording the relative intensity of the transmitted energy on the recorder, and

(4) marking the resulting graph at known wave drum readings.

Scanning the Globar spectrum was accomplished by gear-and-pulley drive of the wave drum from the shaft of a small electric motor. This gear-and-pulley system permitted a variety of scan speeds (2, 1, ½, ¼, and 1/10 wave drum revolution per minute), and allowed the direction of scan to be reversed by crossing the driving belt. Graph marking at known wave drum readings was accomplished by means of a microswitch attached to the amplifier; this microswitch was manually tripped at preselected, visually observed points.

It was decided to attempt wave drum calibration with the system aligned as it would be for experimental vapor dispersion measurements. Calibration runs were made using three different absorbers; atmospheric water and carbon dioxide through polystyrene film, atmospheric water vapor, and ammonia gas /7/. Although these calibration runs

resulted in the identification of some calibration frequencies (in particular, absorption lines of atmospheric water and carbon dioxide through polystyrene film were identified), most of the known absorption lines for both atmospheric water and carbon dioxide and for ammonia gas were masked by background noise. The long optical path resulted in considerable energy loss, with a weakened signal therefore reaching the detector. This signal could be amplified by increasing the gain of the amplifier, but the corresponding amplification of background noise necessitated the use of a slower recorder response time. Increasing the energy intensity by opening the monochrometer exit slit resulted in decreased monochromaticity of the energy reaching the detector. This, plus the slower response time, completely eliminated the fine structure of the absorption graphs, and therefore also eliminated most of the calibration points. The very slow scan speed of 1/10 wave drum revolution per minute was unsuccessfully used in an effort to offset the slow response time. A different calibration procedure, requiring only slight modification of the present system, is therefore described in detail in Section V of this report. This modification greatly reduces the optical path, so that lower amplification of the signal permits a faster response time. It is anticipated that this modification will permit rapid and precise identification of known absorption bands.

During the wave drum calibration runs, the Globar emission spectrum was scanned both from lower to higher and from higher to lower wavelengths. The drum setting at which each of the identified absorption bands appeared differed slightly on runs of opposite direction, the amount of difference depending on scanning speed and recorder response. Therefore, the average of these two wave drum settings was taken as the actual setting for calibration purposes. A monochromator calibration curve (Figure 17) showing wave length vs wave drum setting was plotted using the points obtained in this calibration.

V CONCLUSIONS AND RECOMMENDATIONS

Calibration runs were made by scanning the absorption spectra in both directions.

In analyzing the resulting graphs containing the identified absorption bands, it was found that a definite recorder delay time existed; the recorder reading at any given time did not correspond to the instantaneous wave drum setting. This lag time is a function of both scan speed and response time. The error in calibration resulting from this can be eliminated by averaging the results obtained from the two scanning directions. Previous optical dispersion measurements made with similar equipment and calibrated with a unidirectional scan might, therefore, contain this systematic error, and should be rechecked.

Based on previous work on the optical dispersion of gases using somewhat similar equipment, and based on tests performed on this system (including a tentative calibration), we are confident that this system will operate satisfactorily. However, the following modifications may improve ease of operation and/or accuracy of results.

A major improvement in the ability to locate more absorption bands will result from use of a different configuration for calibration. By removing the plane mirror (M-6, Figure 4) from the monochromator base and attaching a calibrating platform (A) as indicated, the following goals

will be fulfilled:

1. The number of reflections undergone by the beam along the path (thus the reflection losses) will be significantly reduced.
2. The length of the optical path will be greatly reduced minimizing the effect of beam spread.

The above two steps will result in a significant increase in the fraction of incident radiation reaching the detector.

3. As a result of this increased efficiency of detection, narrower monochromator slit apertures can be used while the same intensity is delivered on the detector.
4. It is to be noted that as the monochromator slits are narrowed, the beam leaving the exit slit becomes more monochromatic. Consequently it should be possible to obtain better definition of the spectral fine structure, thus more accurate calibration curves.

An alternative means of obtaining improvement of approximately the same magnitude would be to mount the detector D and the ellipsoidal mirror M-9 in the positions provided on the monochromator chassis, then calibrate the monochromator before installing the collimating mirror M-7. Although this method would yield almost the same results

as that outlined above, it is felt that the inconvenience involved in removing M-7, mounting M-9 and the detector for calibration, then replacing all three for data runs makes this procedure the less desirable of the two.

A possible method of reducing energy losses along the path during data runs would be to remove M-6, M-7, and M-8 (and possibly M-9) from the system entirely; and replace them with a pair of short focal length lenses of suitable material (e.g., of the same material of which the monochromator prism is made, or of IRTRAN 2). The first lens would collimate the beam leaving S-2 for passage through the refractometer, and the second to focus the collimated beam leaving the refractometer either on a detector slit S-3 or directly on the detector. This change would require a method for compensating for the change in focal length of a lens with wave length, but this problem should be a readily solvable. If this modification were effected, it should also decrease energy losses by eliminating some reflections and by shortening the geometrical path length, (reducing losses by scattering and "beam spread"). An increase in energy transmission efficiency of the order of 15 to 20% is expected from the adoption of this modification.

Use of a Lithium flouride prism will improve system resolving power over the range of wavelengths transmitted by IRTRAN 2. However, the added cost of such a prism must be

weighed against the probability of obtaining more accurate results even though the resolution of the LiF prism is reported as an order of magnitude greater than that of the NaCl prism.

This investigation was conducted in a room in which the humidity was not controlled. The NaCl prism was protected from damage by excessive humidity when not in operation by placing an open container filled with dessicant on the monochromator base near the prism, inverting a large bell jar over the prism, and placing a goose-necked desk lamp directly over the bell jar. In addition a 7-watt light bulb was positioned under the monochromator base beneath the prism and was left on at all times. By this procedure, the relative humidity at the prism was maintained at approximately 42% during calibration runs and between 10-12% when not in operation. This method yielded adequate protection for the prism in this case. However, a more reliable system of humidity control requiring less monitoring is desirable. The most satisfactory solution would appear to be humidity control for the entire room, although an adequate alternative might be available.

It was noted that crossing the wave drum drive belt resulted in scanning speed slightly different from that obtained in direct drive. Taking this discrepancy into account when analyzing data is not difficult; however, other workers may

find this slight inconvenience objectionable. In that case, either a pivot mount for the driving motor can be built obviating the necessity for crossing the belt (large O-ring); or a different belt material may allow crossing without introducing this problem.

BIBLIOGRAPHY

1. J. H. Van Vleck, The Theory of Electric and Magnetic Susceptibilities, Oxford University Press, London, 1932

2. S. Kimel, Optical Dispersion of Gases in the Infrared Region, The Weizmann Institute of Science, Rehovoth, Israel, November, 1960.

3. W. C. Eaton and Frederick H. Thomas, Design and Construction of Instrumentation for Investigating the Optical Dispersion of Gases by Infrared Interferometry, U. S. Naval Postgraduate School, Monterey, California, 1959.

4. W. B. Muncie and F. H. Whittemore, Interferometric Observations of the Optical Dispersion of Carbon Dioxide in the Near Infrared, U. S. Naval Postgraduate School, Monterey, California, 1960.

5. W. E. Williams, Applications of Interferometry, Methuen and Co., Ltd., London, 1950.

6. J. K. Robertson, Introduction to Optics, Geometrical and Physical, D. Van Nostrand Co., New York 1954.

7. Instruction Manual, Perkin-Elmer Infrared Equipment, Volumes1, 2, and 3A, The Perkin-Elmer Corp., Norwalk, Conn., 1952.

8. Standard Conversion Tables for L & N Thermocouples, Leeds & Northrup Company, Philadelphia, Pennsylvania.

9. G. Herzberg, Molecular Spectra and Molecular Structure, II. Infrared and Raman Spectra of Polyatomic Molecules, D. Van Nostrand Co., New York, 1945.

10. N. E. Dorsey, Properties of Ordinary Water-Substance, Reinhold Publishing Co., New York, 1940.

11. Harrison, Lord and Loofbourow, Practical Spectroscopy, Prentice-Hall, Inc., New York, 1949.

12. B. Rossi, Optics, Addison-Wesley Publishing Co., Inc., Reading, Mass., 1957.

13. J. C. Slater and N. H. Frank, Electromagetism, McGraw Hill Book Co., Inc., New York, 1947.

14. F. A. Jenkins and H. E. White, Fundamentals of Optics, McGraw-Hill Book Co., Inc., New York, 1950.

15. International Critical Tables, Vol. III, Mc Graw-Hill Co., Inc., New York, 1930.

16. Journal of the Optical Society of America, Vol. 43, No. 11, November 1953.

17. H. L. Hackforth, Infrared Radiation, McGraw-Hill Co., Inc. New York, 1960.

APPENDIX I

Detector Slit Width Determination

The angle between interference principal maxima of a Rayleigh interferometer is given by the expression: /14/

$$d \sin\theta = m\lambda, \quad m = 1$$

for small angles, $\sin\theta \approx \theta$, so $d\theta = \lambda$, $\theta = \frac{\lambda}{d}$

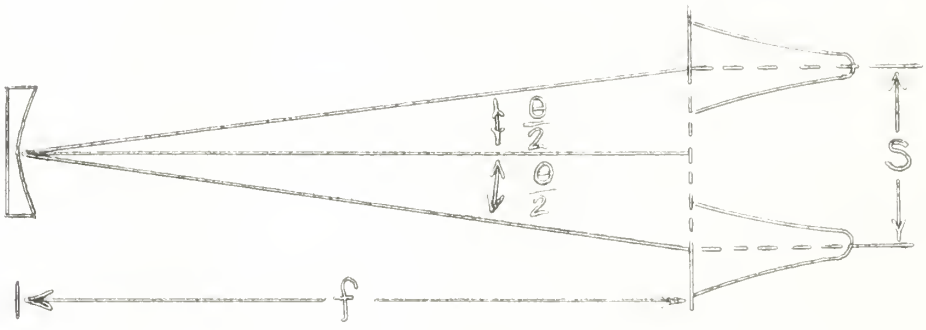

Figure 6. Detector Slit Width Determination

From the geometry of the optical path as seen in Figure 6.

$$\tan\frac{\theta}{2} = \frac{S/g}{f}$$

Again for small angles:

$$\frac{\theta}{2} = \frac{S/2}{f},$$

therefore, for the paraboloidal mirror with a focal length of 267mm., and a slit center to center distance of 6.0mm.,

$$S = \frac{\lambda f}{d} = \frac{267\lambda}{6.0} = 45\lambda$$

This would provide a slit width which would always have the energy equivalent of one principal maximum present.

For closer analytical control, it would be more desirable to limit the size of the slit so that only one, or part of one particular maximum could possibly be in the slit at any one time. This would lead to

$$S \leq \frac{5\lambda}{2} = 22\ \lambda$$

or to an angular half width of principal maxima determination as follows: /14/

$$\delta\theta = \frac{\lambda}{A} = \frac{\lambda}{Nd \cos\theta}$$

again for small angles,

$$\frac{\lambda}{6 \times 6.0 \times 1} = \frac{\lambda}{36}$$

For a focal length of 267mm, this results in a linear half width of

$$\frac{267\lambda}{36} = 7.42\ \lambda$$

Total width of a principal maximum is

$$2 \times 7.42\lambda = 14.84\lambda = 1/3\ S$$

Therefore, the optimum detector slit width should be between 14.8 λ and 22 λ. This range positively eliminates the possibility of any out of phase principal maxima appearing in the slit for an infinitely narrow exit slit of the monochromator. The need for a finite exit slit width alters the optimum detector slit width, since allowances must be made for the additional fringe width formed when the exit slit is opened a finite amount. A geometrical determination indicates that combinations of exit and detector slit widths totalling 45 λ will provide singular detection of the desired maxima. /4/

APPENDIX II

Determination of Slit Width of the Interferometer

In order to have the individual slits of the interferometer as wide as possible, or a low a/d ratio, but at the same time narrow enough to prevent reflection from the sides of the channels, the following determinations were made:

1. The maximum monochromator exit slit width would be 500 microns.
2. The length, L, of the monochromator equals 50cm and the focal length of the paraboloidal mirror is equal to 26.7cm.
3. Width of the channels, D, of the interferometer is 5.0mm.

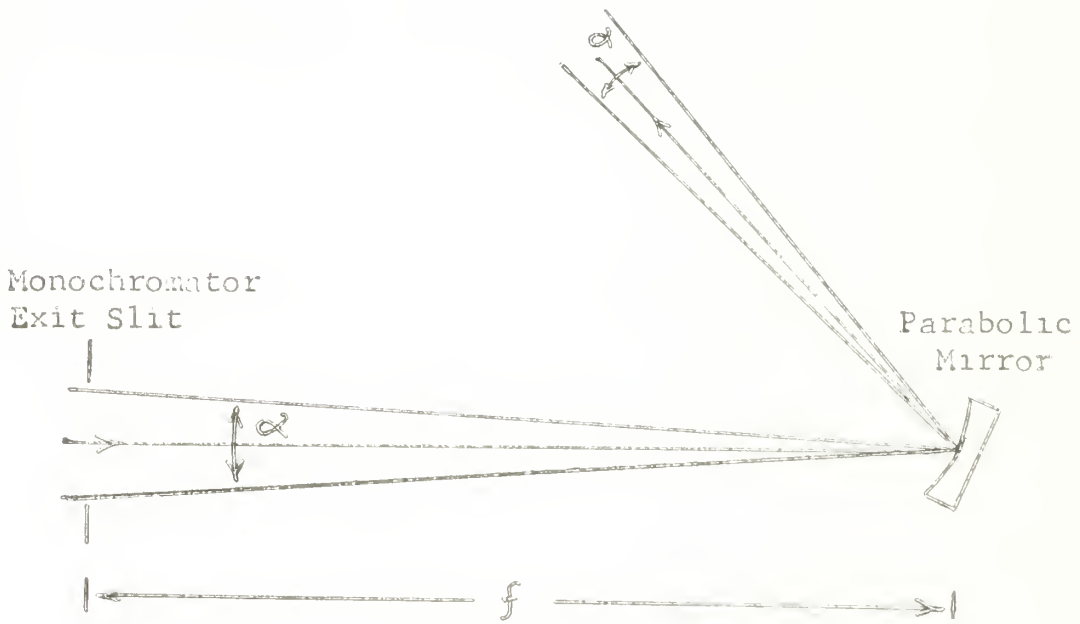

Figure 7. Divergence of Energy due to Exit Slit Width

To determine optimum value of W:

$$\alpha = \frac{2W}{L} = \frac{g}{f}$$

but L = 50cm and g = 0.5mm., therefore,

$$\frac{2W}{50} = \frac{0.5}{26.7}$$

and width of slit of interferometer should be D - 2W or 5.0 - 0.9 = 4.1mm.

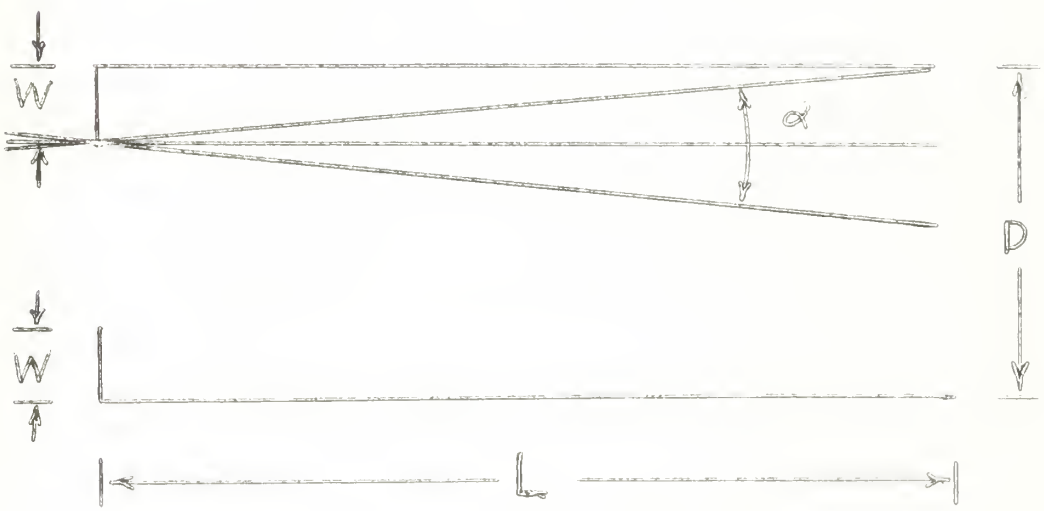

Figure 8. Effect of Divergence of Energy in Interferometer Channel.

or, $R_1 = R_o \frac{\sin N2\gamma}{\sin 2\gamma}$ where N = 3

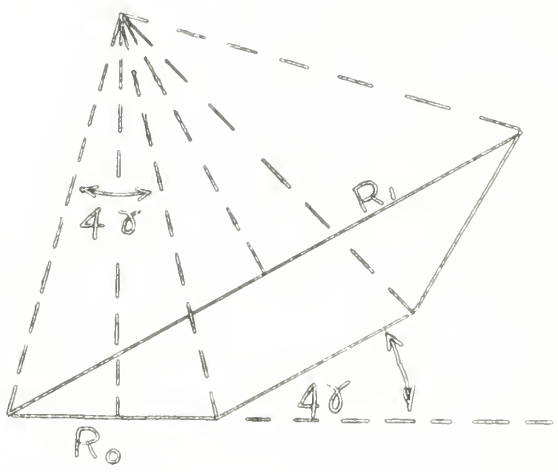

Figure 9. Phase Relationships of Three Alternate Slits

The second set of three slits will be at an angle of 2 from the first set, so we have:

$$2 R_1 \cos\gamma = R$$

Substituting for R_1, we have:

$$2 R_o \frac{\sin N2\gamma}{\sin 2\gamma} \cos\gamma = R$$

Letting R_2 represent the resultant of the alternate channels filled by gas, we have:

$$R = 2 R_o \frac{\sin N\gamma}{\sin 2\gamma} \cos \frac{2\delta + \phi}{2}$$

where ϕ is the phase difference of R_2 caused by the gas.

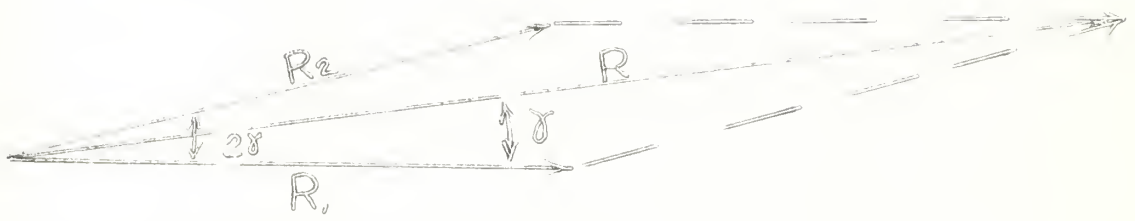

Figure 10. Phase Relationship of Alternate Groups of Three Slits.

For a phase difference of ϕ equal to zero, and a trigonometric substitution of

$$\sin 2\delta = 2 \sin \delta \cos \delta$$

we have:

$$R = R_o \frac{\sin 6\gamma}{\sin \gamma}$$

which is the basic formula for a six slit interference pattern.

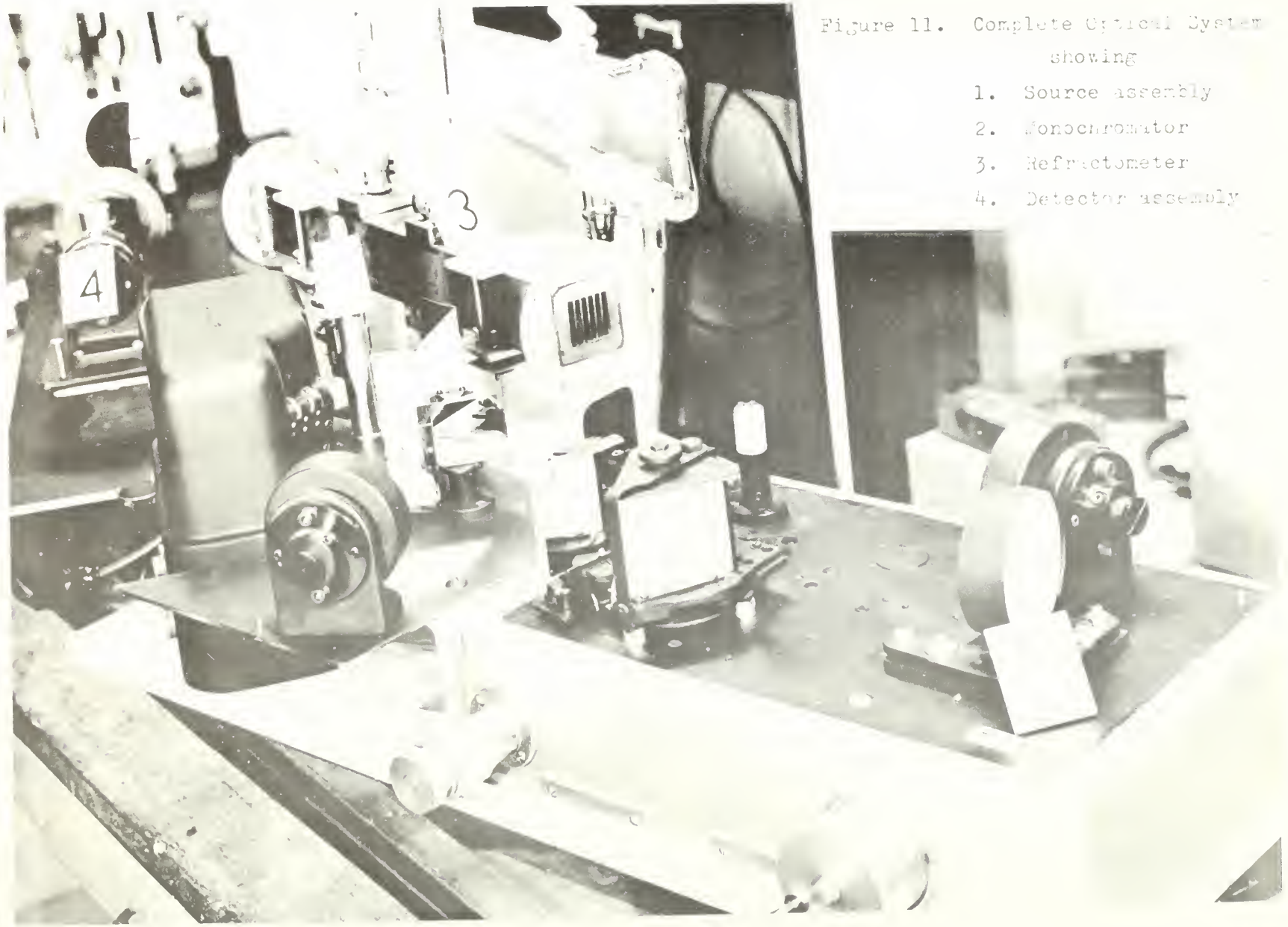

Figure 11. Complete Optical System showing

1. Source assembly
2. Monochromator
3. Refractometer
4. Detector assembly

Figure 12. Source Assembly

1. Globar source
2. Chopper
3. Monochromator

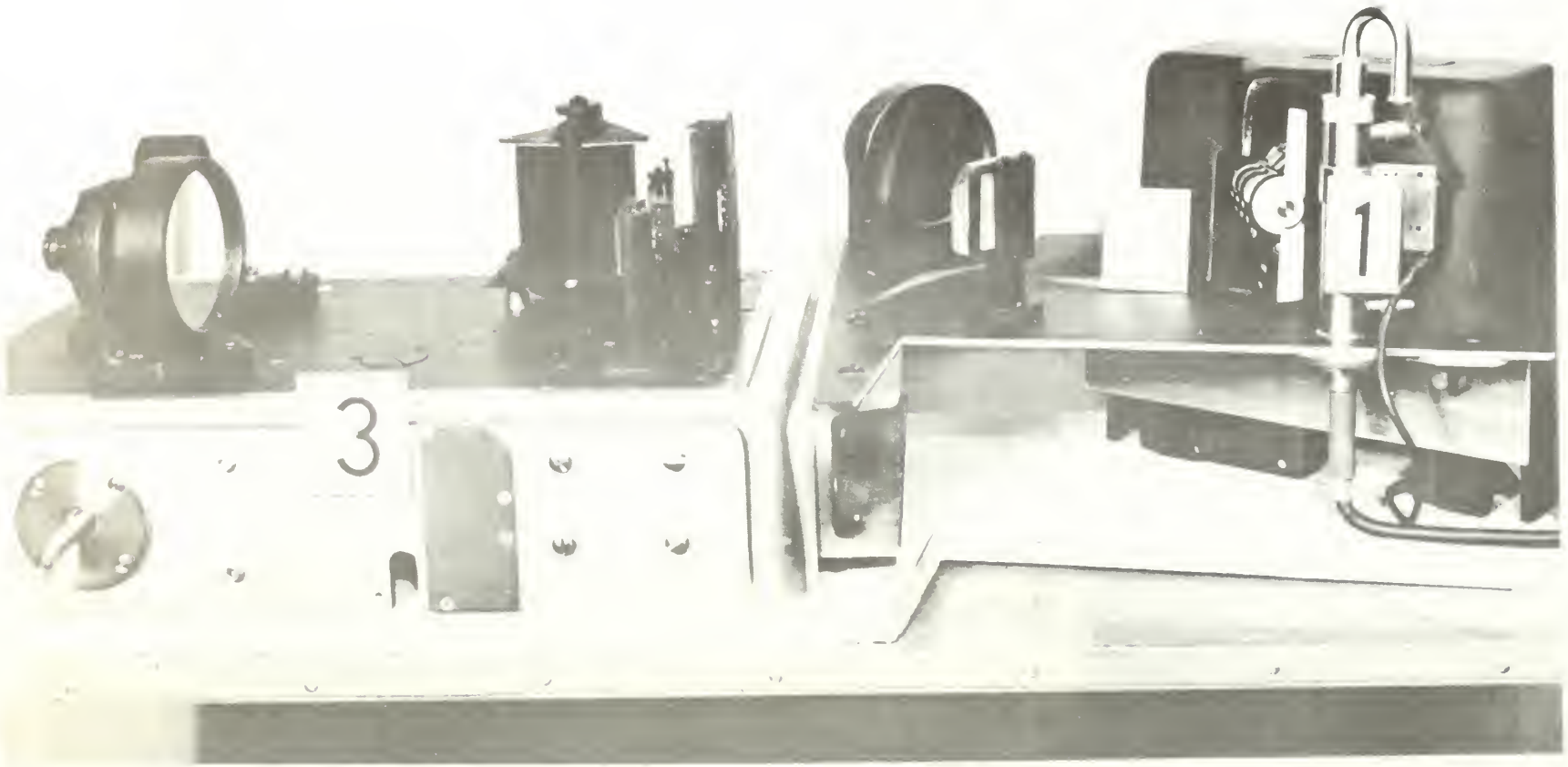

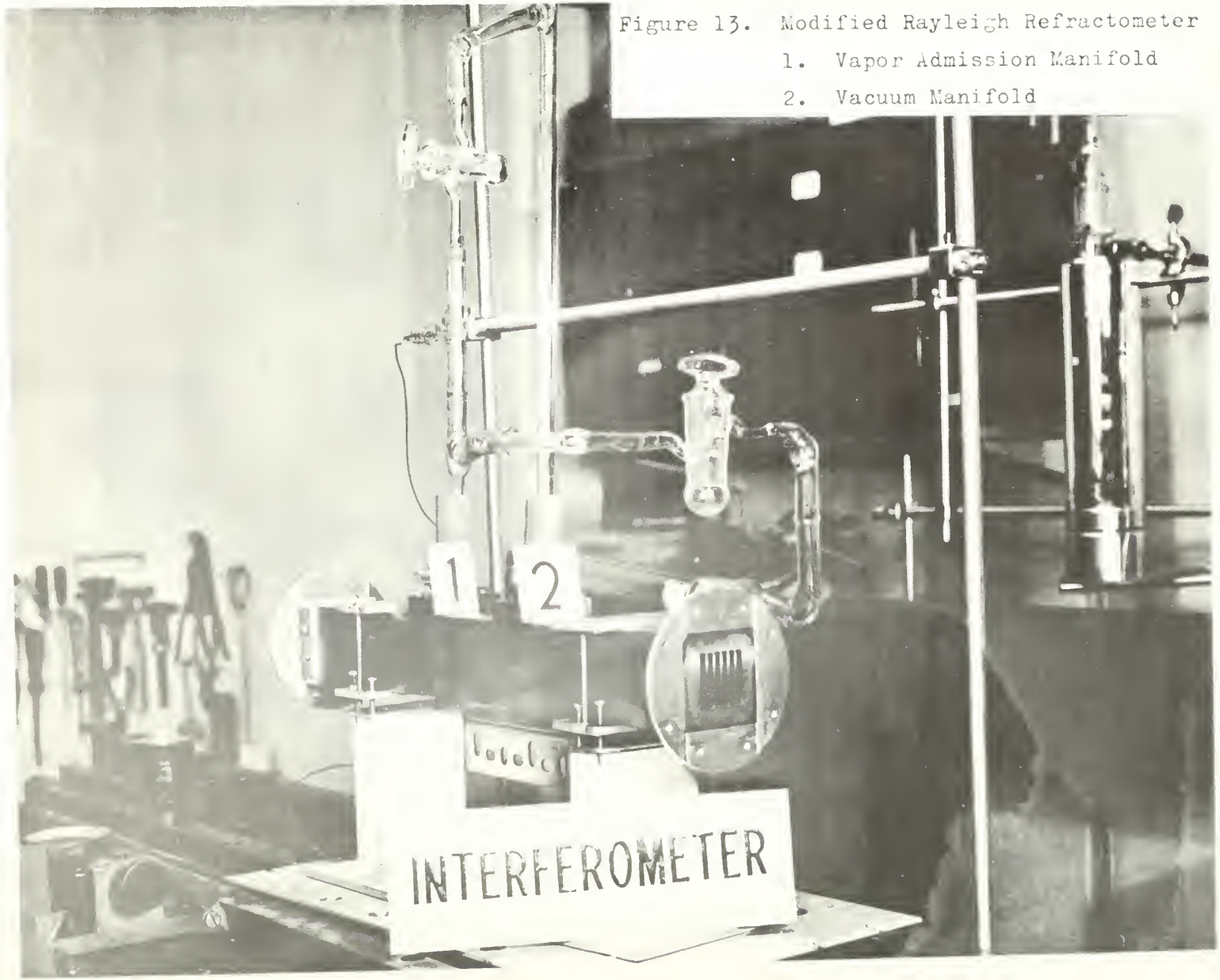

Figure 13. Modified Rayleigh Refractometer
1. Vapor Admission Manifold
2. Vacuum Manifold

Figure 14. Detector Assembly

1. 18°-off-axis parabolic mirror
2. Adjustable detector slit
3. Ellipsoidal mirror and detector

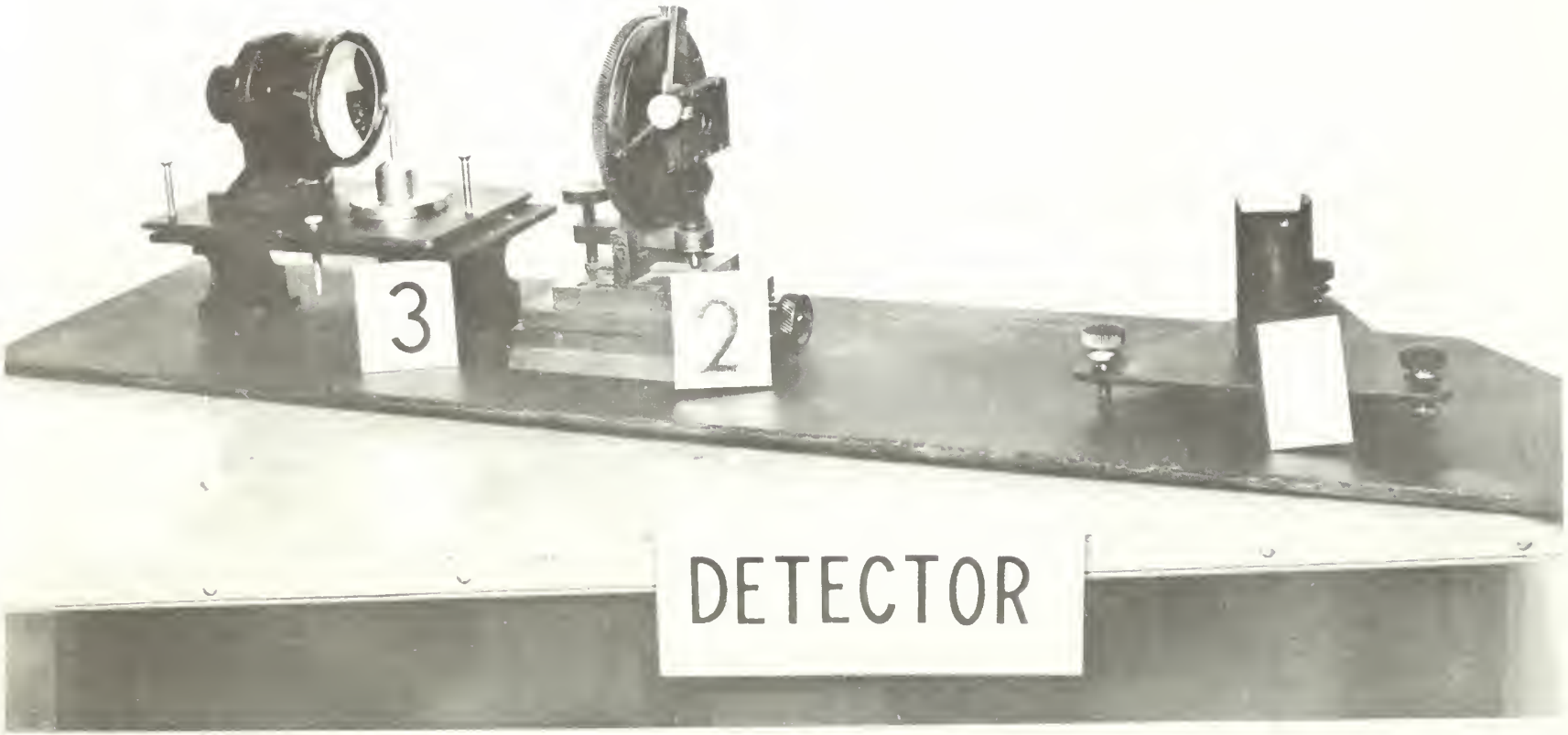

Figure 15. Oven Interior, showing arrangement of heating tapes and water trap

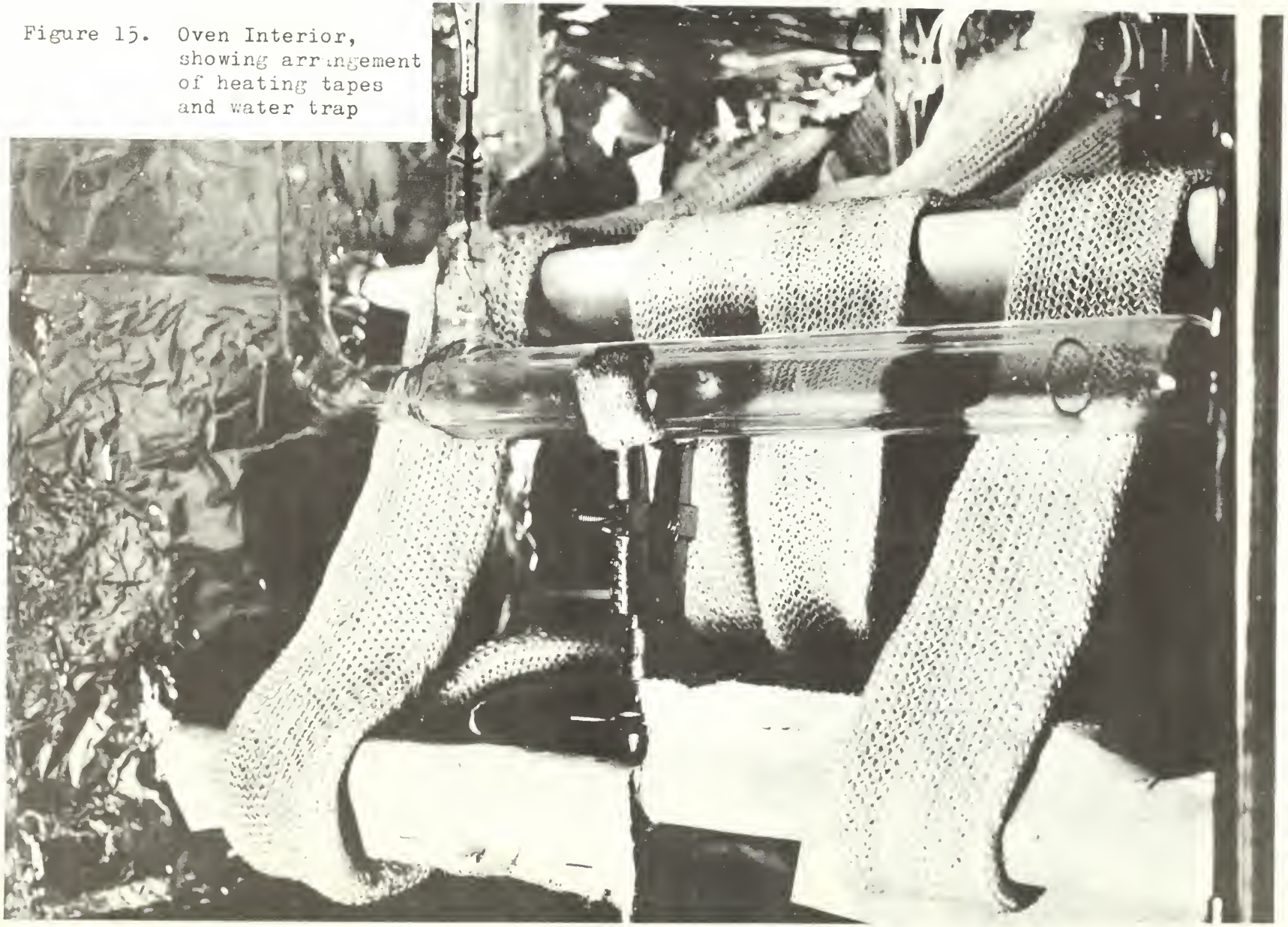

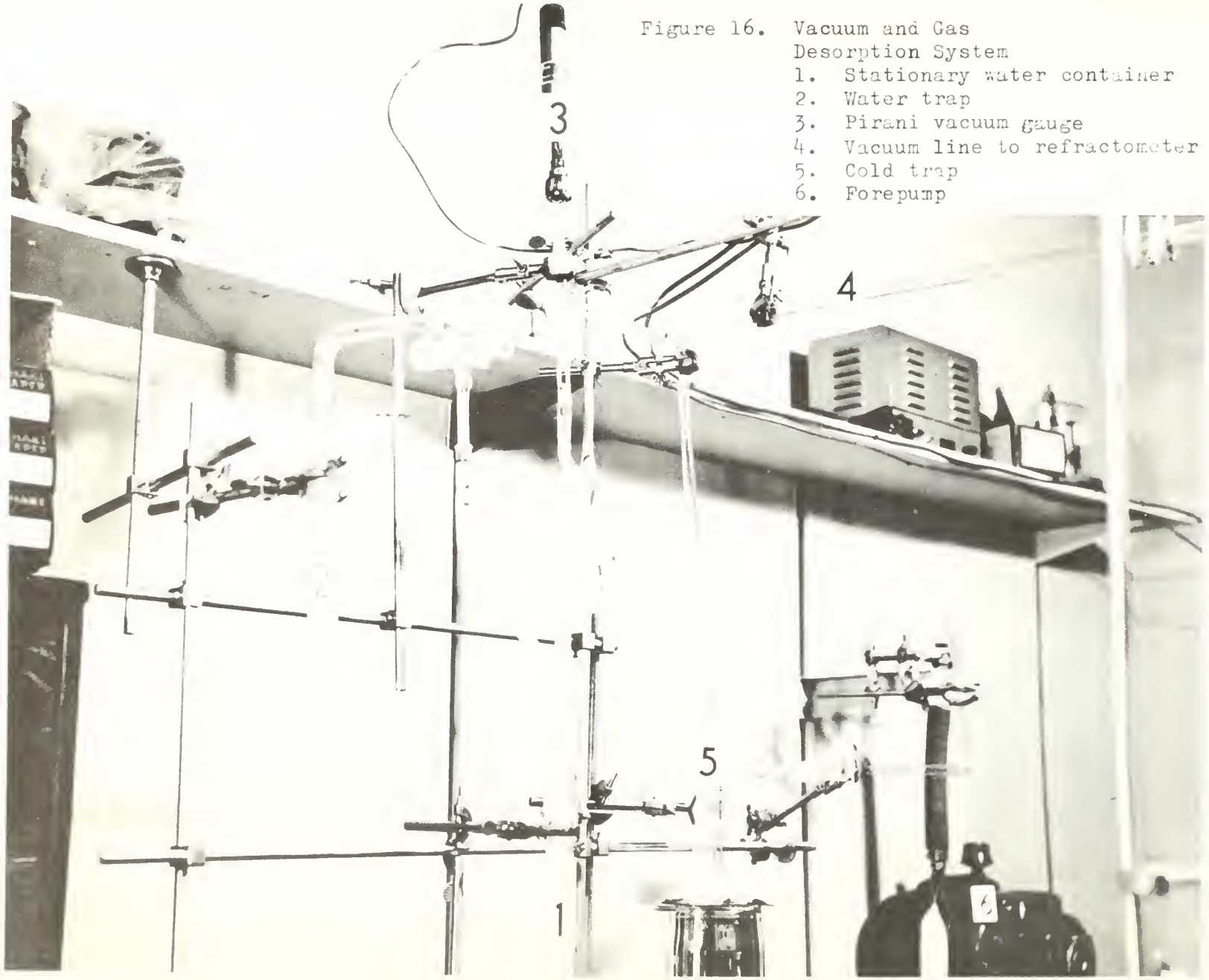

Figure 16. Vacuum and Gas Desorption System
1. Stationary water container
2. Water trap
3. Pirani vacuum gauge
4. Vacuum line to refractometer
5. Cold trap
6. Forepump

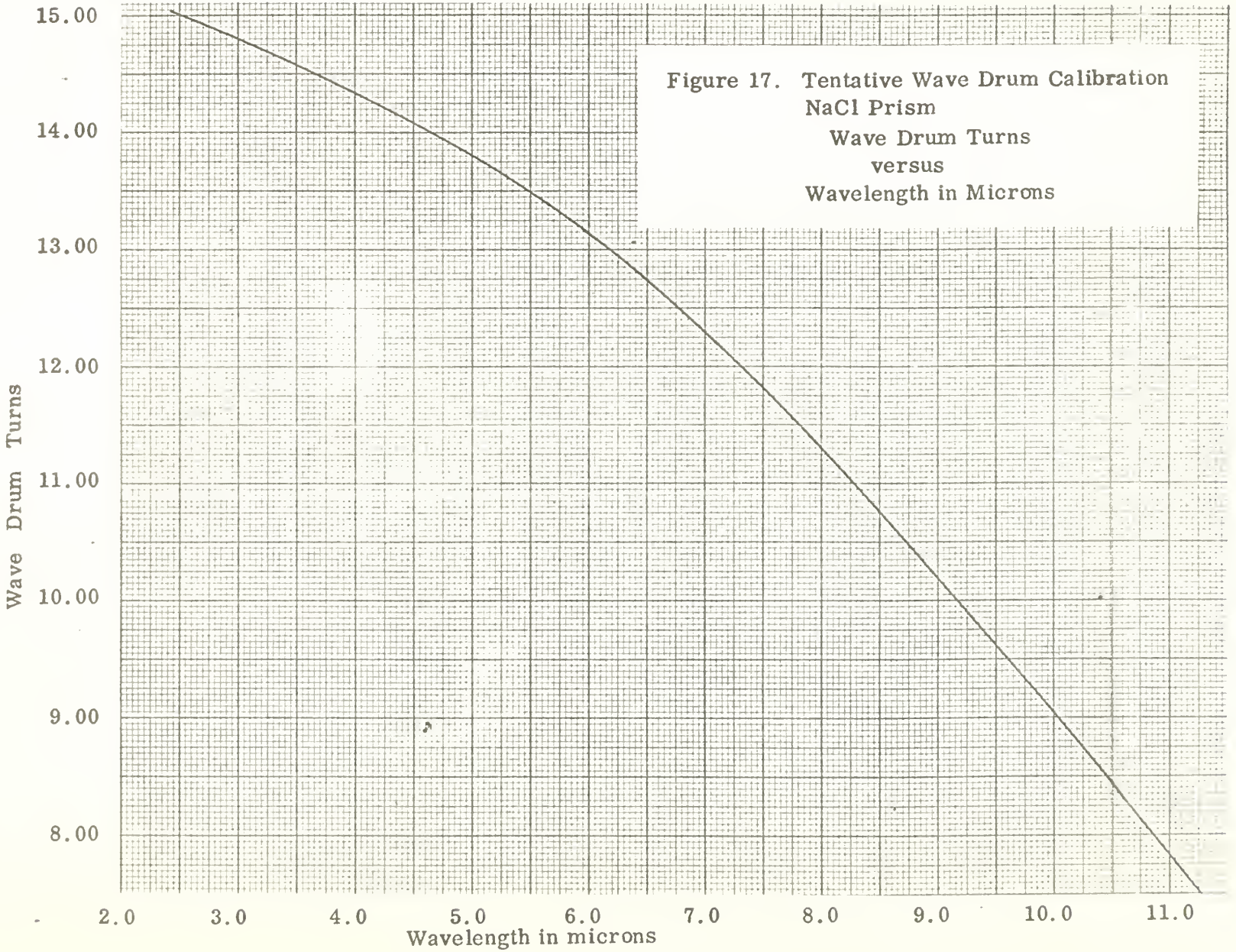

Figure 17. Tentative Wave Drum Calibration
NaCl Prism
Wave Drum Turns
versus
Wavelength in Microns